IMMUNOLOGY

Targeting pulmonary tumor microenvironment with CXCR4-inhibiting nanocomplex to enhance anti–PD-L1 immunotherapy

Zhaoting Li[1], Yixin Wang[1], Yuexin Shen[1], Chenggen Qian[1], David Oupicky[2]*, Minjie Sun[1]*

Anti–programmed cell death 1 ligand 1 (PD-L1) therapy is extraordinarily effective in select patients with cancer. However, insufficient lymphocytic infiltration, weak T cell–induced inflammation, and immunosuppressive cell accumulation in the tumor microenvironment (TME) may greatly diminish the efficacy. Here, we report development of the FX@HP nanocomplex composed of fluorinated polymerized CXCR4 antagonism (FX) and paclitaxel-loaded human serum albumin (HP) for pulmonary delivery of anti–PD-L1 small interfering RNA (siPD-L1) to treat orthotopic lung tumors. FX@HP induced T cell infiltration, increased expression of calreticulin on tumor cells, and reduced the myeloid-derived suppressor cells/regulatory T cells in the TME, thereby acting synergistically with siPD-L1 for effective immunotherapy. Our work suggests that the CXCR4-inhibiting nanocomplex decreases tumor fibrosis, facilitates T cell infiltration and relieves immunosuppression to modulate the immune process to improve the objective response rate of anti–PD-L1 immunotherapy.

INTRODUCTION

Immunotherapy for cancer has made remarkable progress by focusing on blocking T cell immunological checkpoints with chemical small-molecule inhibitors, small interfering RNA (siRNA), or monoclonal antibodies to the programmed cell death 1/programmed cell death 1 ligand 1 (PD-1/PD-L1) receptor/ligand pair and cytotoxic T lymphocyte–associated protein-4 (CTLA-4). Use of such inhibitors has achieved remarkable effects in treating various types of cancers (*1*–*4*). However, the response rate is still limited, with a large fraction of patients failing to respond to the anti–PD-1/PD-L1 immunotherapy. It was reported that insufficient lymphocytic infiltration and T cell–induced inflammation in the tumor microenvironment (TME) may compromise the anti–PD-1/PD-L1 immunotherapy. Moreover, the myeloid-derived suppressor cells (MDSCs) and regulatory T cells (T_{regs}) in the TME inhibit the activation of effector T cells and maintain the immunosuppressive state (*5*–*7*). Efforts to address these problems have become one of the major themes in the field of cancer immunotherapy.

TME is a complex environment for the survival and development of cancer cells, consisting of cellular and noncellular components. Chemokines are the most influential mediators for the establishment and maintenance of TME. Tumors contain a complex chemokine network that controls many of the fundamental properties of the tumor, including immune cell recruitment, angiogenesis, cell migration, and metastasis. Chemokines induce macrophage recruitment into the tumor, thus inhibiting $CD8^+$ T cell immune surveillance and affecting tumor immunity. Chemokines also promote MDSC and T_{reg} infiltration into tumors, aiding in immune evasion (*8*–*10*). Cancer cells from different tumors show different expression of chemokine receptors, but CXCR4 is the most widely expressed in human cancers. The use of a CXCR4 antagonist, AMD3100, in pancreatic cancer increased tumor apoptosis, reduced tumor metastasis, and selectively decreased intratumoral T_{regs}. Exclusion of $CD8^+$ T cells was found in fibroblast- and collagen-rich tumors, suggesting that lack of response of anti–PD-L1 therapy is associated with tumor fibrosis. The CXCL12/CXCR4 axis is closely related to the recruitment of fibrocytes to the lung and the subsequent fibrosis. These facts make CXCR4 a very promising target of cancer immune therapies (*11*–*14*).

In addition to increasing the infiltration of effector T cells and reducing negative immune suppressor cells, close cooperation between dendritic cells (DCs) and T cells is another important step to ensure the immune response process. Chemotherapeutic drugs [i.e., paclitaxel (PTX), doxorubicin, and cisplatin] are reported to activate the immune system and regulate the immunosuppressive TME when used at certain doses (*15*–*17*). These drugs can induce immunogenic cancer cell death to promote tumor antigen release and further presentation by DCs to ultimately activate cytotoxic T lymphocytes (CTLs). Pretreatment with chemotherapeutics makes cancer cells more sensitive to CTL cytotoxicity. Furthermore, we can remodel the tumor immunosuppressive microenvironment by depleting suppressor cells such as T_{regs} and inhibitory cytokines such as interleukin-10 (IL-10) and transforming growth factor–β (TGF-β). It was reported that low-dose PTX modulates cytokine network and inhibits T_{regs} to relieve the immunosuppressive TME. Moreover, low dose of PTX induces calreticulin (CRT) exposure on cancer cells, stimulates DCs, and thus rebuilds the immunosurveillance (*18*–*20*).

Here, we propose a pulmonary delivery strategy to modulate immune response and enhance anti–PD-L1 immunotherapy with the CXCR4 polymeric nanocomplex FX/siPD-L1@HP. On the basis of our CXCR4 research foundation, we encapsulate PTX through human serum albumin (HSA), then attach the fluorinated FX to the HP surface, and pack siPD-L1 layer by layer to form our nanocomplex for the treatment of Lewis lung carcinoma (LLC) and lung metastasis of breast cancer (LMBC) (Fig. 1, A and B). We found that the designed CXCR4 antagonism polymer FX decreased tumor fibrosis in the anti–PD-L1–resistant tumor to increase CTL infiltration and overcome immune exclusion. We also show that not only the CXCR4 antagonist part of the nanocomplex could inhibit T_{regs} and MDSCs, which was synergistic with the PD-L1 silence treatment,

[1]State Key Laboratory of Natural Medicines, Department of Pharmaceutics, China Pharmaceutical University, Nanjing 210009, China. [2]Center for Drug Delivery and Nanomedicine, Department of Pharmaceutical Sciences, University of Nebraska Medical Center, Omaha, NE 68198, USA.
*Corresponding author. Email: david.oupicky@unmc.edu (D.O.); msun@cpu.edu.cn (M.S.)

but also simultaneous low-dose PTX could promote CRT exposure and increase the sensitivity of tumor cells to CTL killing.

RESULTS

Preparation and characterization of the FX@HP nanocomplex

We first synthesized a new fluorinated bioreducible polymer (FX) with CXCR4 antagonistic activity using a synthetic procedure (fig. S1) as previously reported (*21*–*23*). Representative ^{1}H-NMR (proton nuclear magnetic resonance) spectra of the polymer showed characteristic aromatic phenylene protons of the cyclam monomer at 7.4 to 7.8 parts per million (fig. S2). FX had M_W = 5300 (Đ = 1.15) with 3.2% fluorine content as determined by elemental analysis. Inspired by the commercial Abraxane, we encapsulated a low dose of PTX in HSA to form HP nanoparticles with zeta potential about −14 mV and hydrodynamic diameter ~110 nm. PTX was entrapped in the hydrophobic cavity of HSA to form HP, which was accomplished using dithiothreitol (DTT) to regulate the disulfide bond of HSA. Then, the FX was mixed with the HP nanoparticles through electrostatic interactions to form FX@HP. The final preparation also included electrostatically adsorbed siRNA to form FX/siRNA@HP, which showed nanocomplex with spherical structure under a transmission electron microscope (TEM) (Fig. 2A). The particle size of FX@HP was about 160 nm, and the zeta potential was 37 mV. After siRNA binding, the particle size decreased slightly to 150 nm and the zeta potential decreased to 12 mV. At w/w 5 (FX versus siRNA), the particle size of FX/siRNA was about 90 nm, and the zeta potential was about 21 mV (Fig. 2, B and C).

The FX polymer used in the preparation of the particles contained reducible disulfide bonds. We thus evaluated how disulfide reduction affects the release of the active components (PTX and siRNA) from the particles. First, in the RNA agarose gel electrophoresis in Fig. 2D, the glutathione (GSH) treatment caused the release of free siRNA from the particles. Similarly, the in vitro PTX release was measured and shown in Fig. 2E. Incubation with 10-mmol GSH resulted in a notably increased rate of PTX release. The cellular uptake of nanocomplex carrying carboxyfluorescein (FAM)–siRNA was measured by flow cytometry. RX/FAM-siRNA was poorly internalized by the cells, whereas the uptake of FX/FAM-siRNA and FX/FAM-siRNA@HP was significantly increased because of the fluorination effect (Fig. 2F). We reasoned that the uptake enhancement may result from enhanced interaction between cell membrane and nanocomplex because of fluorine modification (*24*).

PD-L1 silencing, CXCR4 antagonism, and in vitro immune activation of the nanocomplex

The CXCR4 antagonism ability of the nanocomplex was detected based on the inhibition of stromal sell-derived factor-1(SDF-1)–induced CXCR4-EGFP redistribution. Compared with the positive control

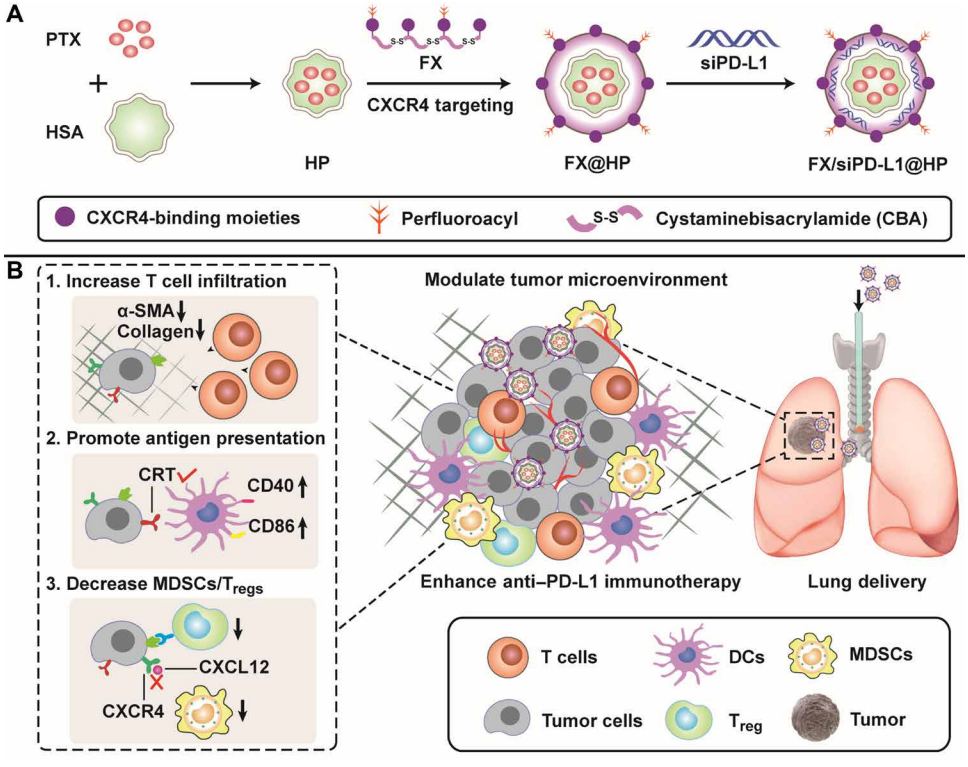

Fig. 1. Preparation and immune activation mechanism of FX/siPD-L1@HP. (**A**) Preparation of FX/siPD-L1@HP. PTX was encapsulated in HSA to obtain HP as a core of the nanocomplex and FX was wrapped on the outer layer of HP forming FX@HP. The final preparation FX/siPD-L1@HP is formed by electrostatic adsorption of siRNA. (**B**) FX/siPD-L1@HP was administered by pulmonary delivery and modulates TME to enhance anti–PD-L1 immunotherapy through three pathways. First, FX/siPD-L1@HP can decrease α-SMA and collagen expression to attenuate fibrosis in tumors, which will facilitate T cell infiltration. Second, low dosage of PTX can expose the CRT proteins on the surface of tumor cells, thus promoting the maturation and antigen presentation of DCs. Third, the released PTX and CXCR4 antagonism effect can reduce the MDSCs and T_{regs}, thereby relieving the immunosuppressive state in the TME.

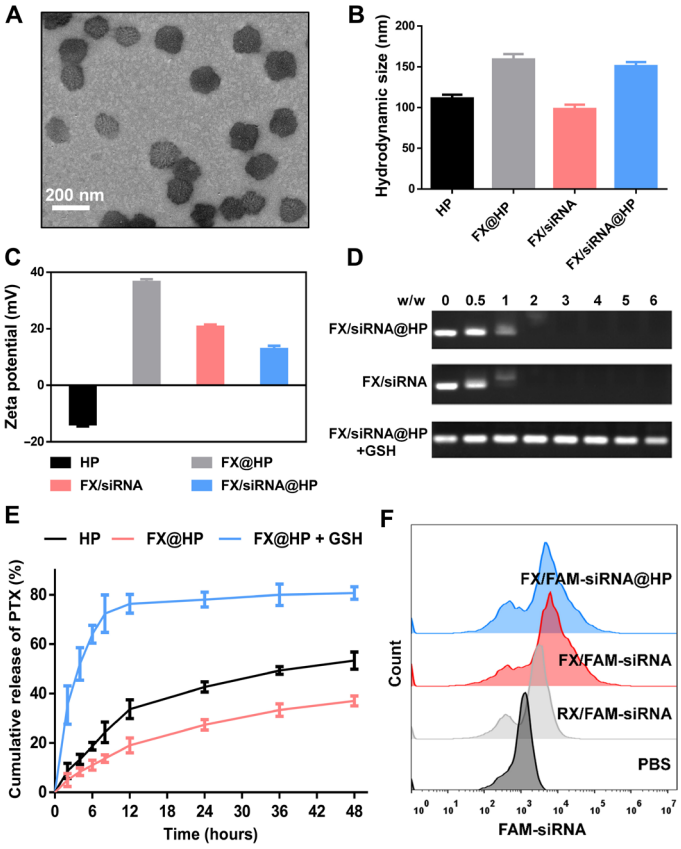

Fig. 2. Physicochemical characterization of the nanoparticles. (**A**) TEM image of FX/siRNA@HP. (**B**) Hydrodynamic size and (**C**) zeta potential of the nanocomplex. (**D**) siRNA condensation by the nanocomplex and release of siRNA from the nanocomplex treated with GSH. (**E**) In vitro cumulative release profiles of PTX released from the nanocomplex. (**F**) Cell uptake determined by flow cytometry at 4 hours after incubation with the FAM-siRNA nanocomplex in LLC cells.

AMD3100, our nanocomplex showed similar CXCR4 antagonism effect, whereas the control polyethyleneimine (PEI) did not antagonize CXCR4 (Fig. 3A). For anti–PD-L1 therapy, it is important to test the PD-L1 silencing ability of the nanocomplex in LLC cells in vitro. It was shown that FX/siPD-L1@HP and FX/siPD-L1 silenced the PD-L1 expression better than RX/siPD-L1 because of improved cell uptake (Fig. 3B).

DCs are the most powerful professional antigen-presenting cells (APCs) in the immune process. They can efficiently absorb, process, and present antigens. Mature DCs can activate the initial T cells effectively and are at the center of initiating, regulating, and maintaining the immune response. CRT expression level is an important indicator of immune activation and therapeutic effect in lung cancer (*25*). The CRT exposure on tumor cells was detected by the confocal assay and flow cytometry assay. As shown in Fig. 3C, LLC cells treated with phosphate-buffered saline (PBS), PEI/siPD-L1, and FX/siPD-L1 showed few CRT expression, but significantly more CRT expression was observed in the FX/siScr@HP and FX/siPD-L1@HP group. From the flow cytometry assay, we found that the CRT expression increased from 4.59% (PBS) to 41.3% after FX/siPD-L1@HP treatment, which was consistent with the confocal observation (Fig. 3D). To test whether the nanocomplex-induced CRT exposure will enhance activation of DCs, the expression of CD40 and CD86 in DCs after different treatments was detected by flow cytometry. It was found that FX/siPD-L1@HP treatment induced higher levels of CD86 and CD40 up-regulation on the DCs, representing the maturation of DCs (Fig. 3, E and F). The FX/siPD-L1@HP nanocomplex promoted CRT exposure on tumor cells and thereby further enhanced the antigen presentation and maturation of DCs to modulate the immune process.

Biodistribution and antitumor efficacy of the nanocomplex in orthotopic LLC

Failure to effectively reach the tumor and deficient interaction with the TME account for poor immunotherapeutic effect. Here, we used fluorescence imaging to analyze the biodistribution of the nanocomplex in vivo. FX@HP was prepared with Cy5-siRNA and administered by intratracheal instillation in the mice with orthotopic LLC. Near-infrared images of the mice were taken at different time points from 1 to 24 hours (Fig. 4A). It was found that, at 1 hour, fluorescence mainly concentrated in the lungs, and with the metabolism, 12 hours later, fluorescence appeared in the abdominal cavity. We found that, at 24 hours, there was still strong fluorescence in the lung. From the anatomical results, our preparations were well distributed in the lungs at 1, 12, and 24 hours (Fig. 4B). At 24 hours, the red spot in the lung indicates the strongest fluorescence in the lung tumor, proving that the PD-L1 inhibitors given by pulmonary delivery are well distributed in the microenvironment of the lung tumor. The fluorescence intensity of each organ was statistically analyzed (Fig. 4C), and it is found that the fluorescence intensity of the lung is far higher than that of other tissues and organs, which will ensure the interaction of the nanocomplex with the TME and provide a guarantee for adequate immune regulation.

High expression of SDF-1/CXCR4 has been reported in lung cancer, which is associated with poor therapeutic effect and prognosis (*26*). Immunofluorescence analysis of the lung tumors showed strong CXCR4 expression on day 8 (Fig. 4D). The mice were administered on days 8, 10, 12, and 14 by pulmonary delivery, and the lungs were harvested for hematoxylin and eosin (H&E) assay on day 16 (Fig. 4E). As shown in Fig. 4F, the lung tumors in the untreated group grew well, whereas the tumors in the FX/siPD-L1@HP–treated group were greatly reduced and necrotic. In addition, FX/siScr or PEI/siPD-L1 only showed moderate effect on tumor inhibition. Two additional administrations were given on days 16 and 18, and the survival time was monitored until day 60. Although the PD-L1 silence treatment (PEI/siPD-L1) showed limited survival prolongation effect, the nanocomplex FX/siPD-L1@HP showed its superiority and prolonged the median survival from 25.5 days (untreated) to 55 days (Fig. 4G). Similarly, increased survival was also observed after FX/siScr@HP treatment (37.5 days). We found that the combination of CXCR4 antagonism and PD-L1 inhibition in FX/siPD-L1 (median survival, 47 days) showed significantly better therapeutic effect than either treatment alone (PEI/siPD-L1, 35.5 days; FX/siScr, 32 days).

Antitumor efficacy of the nanocomplex in LMBC

Metastatic breast cancers are largely resistant to immune checkpoint blockade (ICB) therapy, and the lung metastasis model was established by intravenous injection of 4T1-Luc cells to test the antitumor efficacy of the nanocomplex in vivo (Fig. 5A). By luciferase imaging, it was found that obvious lung metastases were formed on day 8. After different treatments, as shown in Fig. 5B, only moderate antimetastasis effect was observed in the PEI/siPD-L1 group, whereas

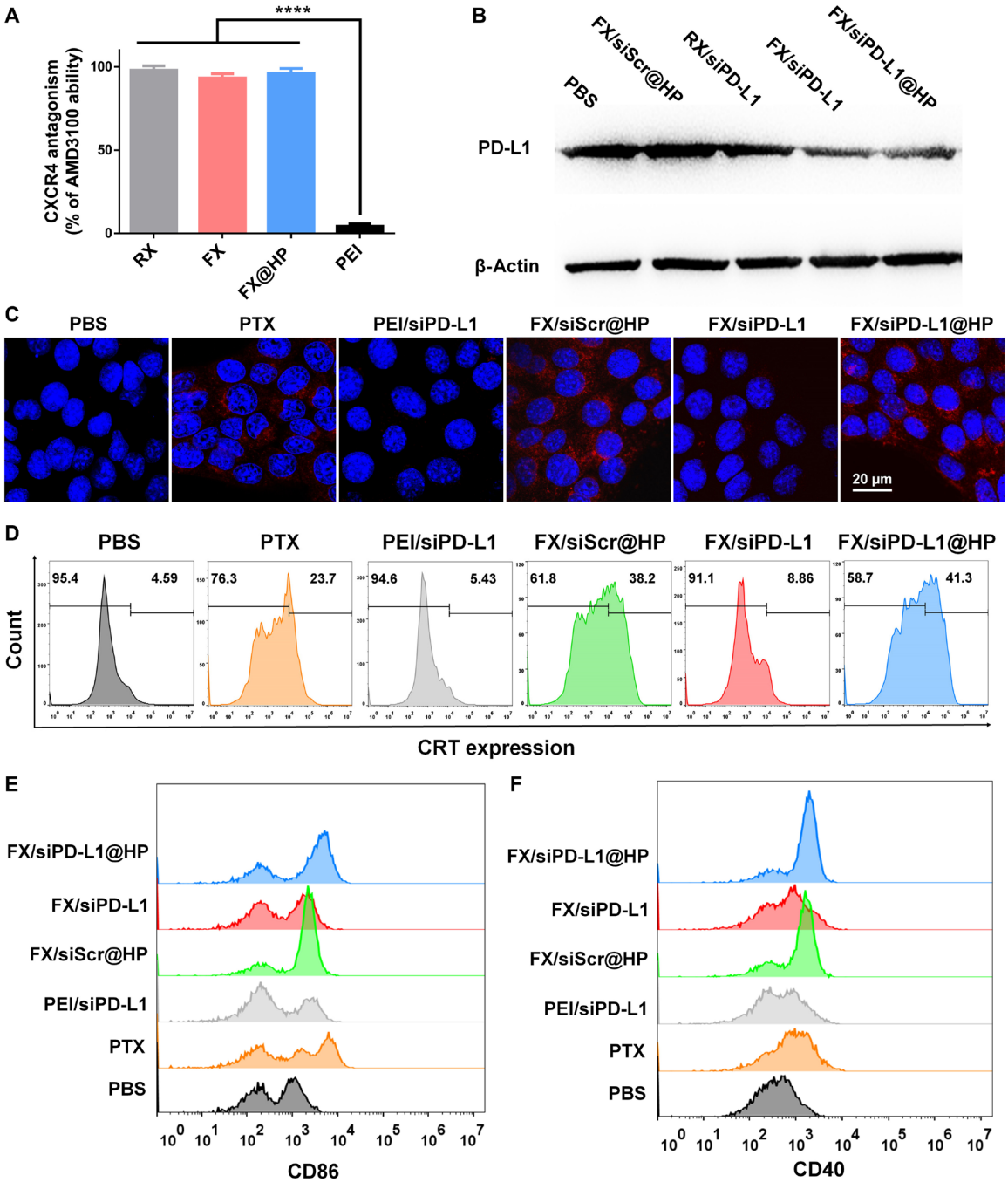

Fig. 3. In vitro immune activation. (**A**) CXCR4 antagonism ability of the nanocomplex relative to AMD3100. Data were analyzed with unpaired *t* test (****$P < 0.0001$ versus PEI). (**B**) PD-L1 gene silence by the nanocomplex (100 nM siPD-L1) in vitro. (**C**) Expression of CRT on LLC cells treated with PBS, free PTX, PEI/siPD-L1, FX/siScr@HP, FX/siPD-L1, and FX/siPD-L1@HP (100 nM PTX and 100 nM siPD-L1). (**D**) Flow cytometry assay of CRT expression on LLC cells after different treatments. Expression of (**E**) CD86 and (**F**) CD40 of $CD11c^+$ BMDCs after coculturing with LLC cells with different treatments.

FX/siPD-L1 showed robust tumor inhibition, indicating the important role of CXCR4 antagonism in anti–PD-L1 therapy. The weakest bioluminescence intensity in FX/siPD-L1@HP represents the best antitumor efficacy. Three mice were euthanized on day 16, and lungs were harvested for H&E assay. It was shown that the number and size of lung metastases in the FX/siPD-L1@HP treatment group are much smaller than those in the PEI/siPD-L1 treatment group (Fig. 5, C and D), consistent with the results of the bioluminescence observation. Furthermore, the survival time of mice after the FX/siPD-L1 treatment was significantly increased compared with PEI/siPD-L1 treatment. PD-L1 blocking therapy only prolonged the median survival from 20 to 27.5 days, whereas FX/siPD-L1@HP

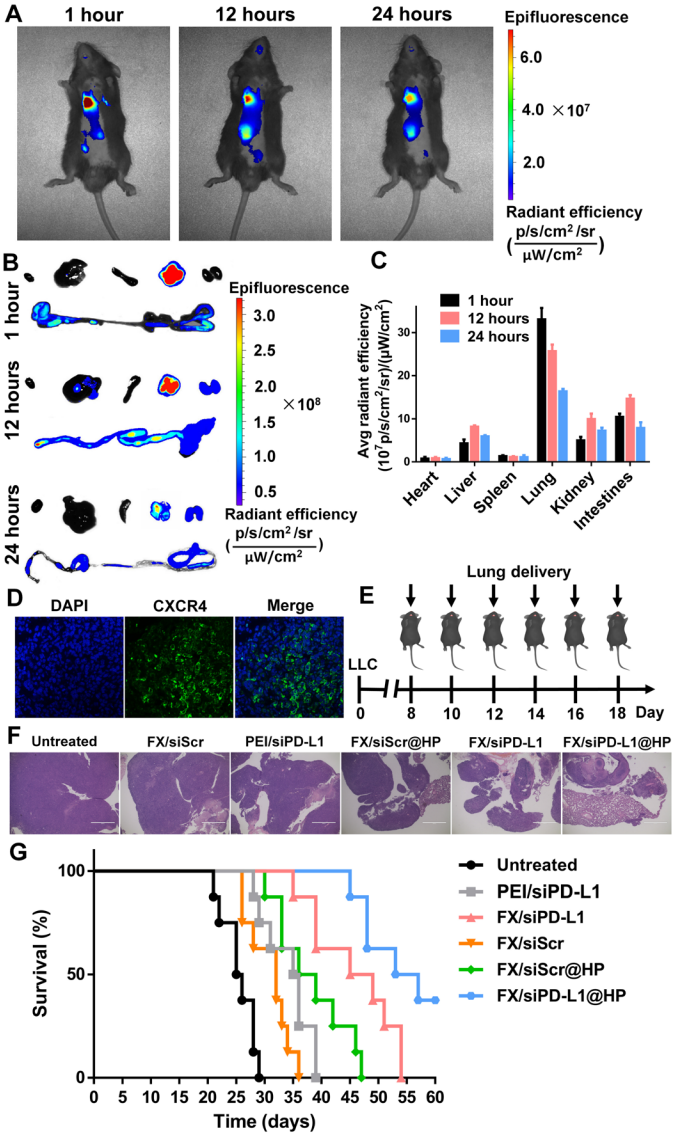

Fig. 4. Biodistribution and antitumor efficacy of the nanocomplex in orthotopic LLC in vivo. (**A**) In vivo fluorescence imaging at different times after pulmonary delivery of the nanocomplex. (**B**) Ex vivo fluorescence images of major organs at 1, 12, and 24 hours. From left to right, heart, liver, spleen, lung, kidney, and intestines. (**C**) Organ distribution of siRNA-Cy5 based on ex vivo fluorescence intensity. (**D**) CXCR4 expression in LLC on day 8. (**E**) Schematic illustrating the in vivo treatments of the LLC-bearing mice. (**F**) H&E assay of the lung tumor after different treatments on day 16. (**G**) Mice were treated with the nanocomplex on days 8, 10, 12, 14, 16, and 18, and survivals were monitored to day 60 ($n = 8$). Data were analyzed with log-rank test: FX/siPD-L1 versus PEI/siPD-L1 ($P = 0.0040$); FX/siPD-L1@HP versus PEI/siPD-L1 ($P < 0.0001$).

prolonged the median survival to 53 days (Fig. 5E). These results suggest that the nanocomplex could significantly enhance the anti–PD-L1 therapy in the treatment of LMBC.

In vivo antitumor mechanism

To investigate the antitumor mechanism, the LLC model was established, and after four times administration, the tumors were harvested for further analysis (Fig. 6A). More CRT exposure on cancer cells was associated with more infiltration of mature DCs and effector memory T cells, indicating that CRT triggers the activation of immune responses in the TME to prolong the survival of patients with non–small cell lung cancer (NSCLC) (*25*). Therefore, we can promote the exposure of CRT protein on the surface of cancer cells by a low dosage of PTX, which is beneficial to the activation of DCs and increases the sensitivity of tumor cells to the killing of CTLs. As shown in Fig. 6B, the CRT expression increased from 13.8% (untreated) to 38.7% after treatment with FX/siPD-L1@HP. The CRT exposure on cancer cells was caused by the released PTX from the nanocomplex, sending the "eat-me" signal and stimulating the phagocytosis of these cancer cells by DCs (*27*). Consequently, the antigen presentation and maturation of DCs were enhanced, inducing the further intensive activation and tumor cell killing ability of CTLs.

Adequate T cell infiltration is one of the determinants of improving the response rate of anti–PD-L1 therapy. Although the in vivo PD-L1 silencing effects of PEI/siPD-L1, FX/siPD-L1, and FX/siPD-L1@HP are similar (fig. S3), the antitumor effects of the latter two are far superior to that of the first. We hypothesized that CXCR4 blockade achieved by the CXCR4 antagonistic polymers FX will facilitate T cell infiltration into the tumors to enhance the anti–PD-L1 therapy. The infiltration of $CD8^+$ T cells was analyzed by immunofluorescence staining. Compared with the untreated group, PEI/siPD-L1 slightly increased the infiltration of $CD8^+$ T cells into tumor as a result of silencing the expression of PD-L1, likely because blocking PD-L1 increased the proliferation and activation of T cells (fig. S4). Significantly more $CD8^+$ T cells were observed in the FX/siPD-L1@HP– and FX/siPD-L1–treated groups than in the PEI/siPD-L1 group, indicating that blocking CXCR4 effectively increased T cell infiltration (Fig. 6, C and D). We further found that blocking CXCR4 by the nanocomplex could significantly down-regulate the expression of α-smooth muscle actin (α-SMA) and collagen, thus attenuating the fibrosis of tumors and immune exclusion phenomenon (Fig. 6E). It was found that decreasing the fibrosis of tumors by CXCR4 inhibition will increase T cell infiltration to enhance the anti–PD-L1 therapy.

MDSCs, with expression of two surface markers CD11b and Gr-1, are a group of heterogeneous cells derived from bone marrow, also known as precursors of DCs, macrophages, or granulocytes. They have the remarkable ability of suppressing immune cell responses. Concomitantly, $Foxp3^+$ T_{regs} also show immunosuppressive effects in the TME, usually inhibiting or down-regulating the induction and proliferation of $CD8^+$ T cells (*28*–*31*). We demonstrated that the CXCR4 antagonistic polymer FX and released low-dose PTX could inhibit T_{regs} and MDSCs in the TME to relieve the immunosuppressive state. For the T_{regs}, with the treatment of FX/siPD-L1@HP, Foxp3 expression was ~13.8% significantly lower than that of PEI/siPD-L1 (~37.8%), which proves that compared with simple PD-L1 silencing, our combination nanocomplex can better eliminate immune suppression by inhibiting negative immunomodulatory cells in TME (Fig. 6, F and G). As shown in Fig. 6 (H and I), the $CD11b^+$ $Gr1^+$ cells were high at ~66.4% in the untreated LLC tumors. It was found that although the silencing of PD-L1 had a weak effect on decreasing the MDSCs, FX/siPD-L1@HP could significantly reduce MDSCs in the TME. Therefore, we could conclude that the released PTX and CXCR4 antagonism polymer (FX) could enhance the anti–PD-L1 immunotherapy by decreasing the T_{regs} and MDSCs. Analysis of the expression of interferon-γ (IFN-γ) and tumor necrosis factor–α (TNFα) (Fig. 6, J and K) showed significantly better activation of immune cells in the FX/siPD-L1@HP group than in the

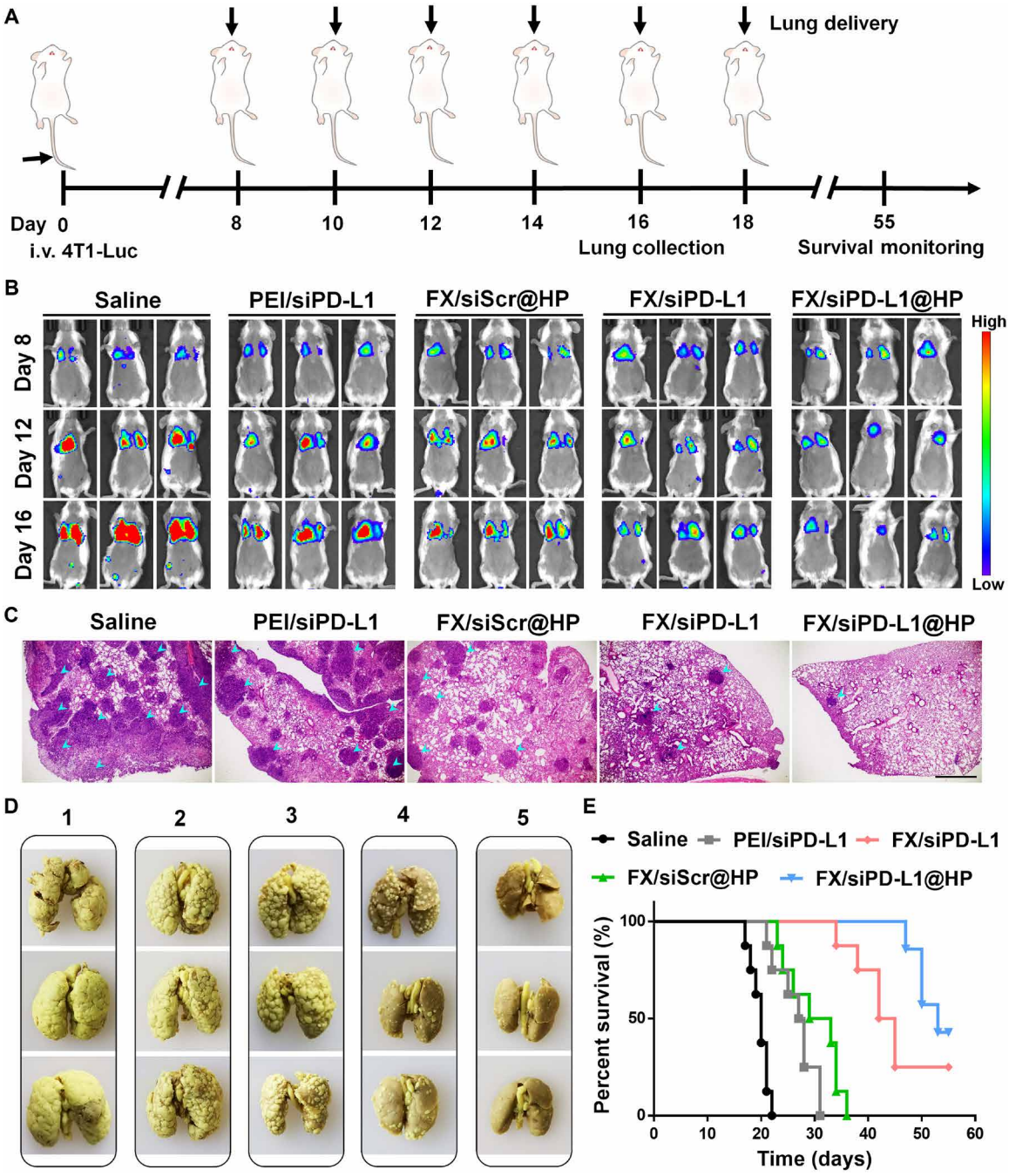

Fig. 5. Antitumor efficacy of the nanocomplex in LMBC in vivo. (**A**) Schematic illustrating the in vivo treatments of the LMBC-bearing mice. (**B**) In vivo bioluminescence imaging of the mice bearing LMBC after different treatments. (**C**) H&E assay of the harvested lungs on day 16 (scale bar, 1 mm). (**D**) Representative photographs of the lungs after different treatments on day 16. (1) Untreated, (2) PEI/siPD-L1, (3) FX/siScr@HP, (4) FX/siPD-L1, and (5) FX/siPD-L1@HP. (**E**) Survival curves after different treatments ($n = 8$). Data were analyzed with log-rank test. Median survival: untreated (20 days), PEI/siPD-L1 (27.5 days), FX/siScr@HP (31 days), FX/siPD-L1 (43.5 days), and FX/siPD-L1@HP (53 days).

PEI/siPD-L1 group, thus achieving greater tumor inhibition and longer survival time. Furthermore, we found that the TME expression of IL-10 and TGF-β in the FX/siPD-L1@HP group was much lower than that in the PEI/siPD-L1 group (Fig. 6, L and M, and figs. S5 and S6), which showed that the immunosuppressive state was remarkably suppressed after combined CXCR4 and PD-L1 inhibition.

DISCUSSION

In recent years, anti–PD-1/PD-L1 immunotherapy has attracted great attention and expectations, which is in the center of the spotlight of anticancer immunotherapy (*32*). Despite encouraging progress, only a limited fraction of the patients respond to the anti–PD-1/PD-L1 immunotherapy. Less T cell infiltration in tumors has always

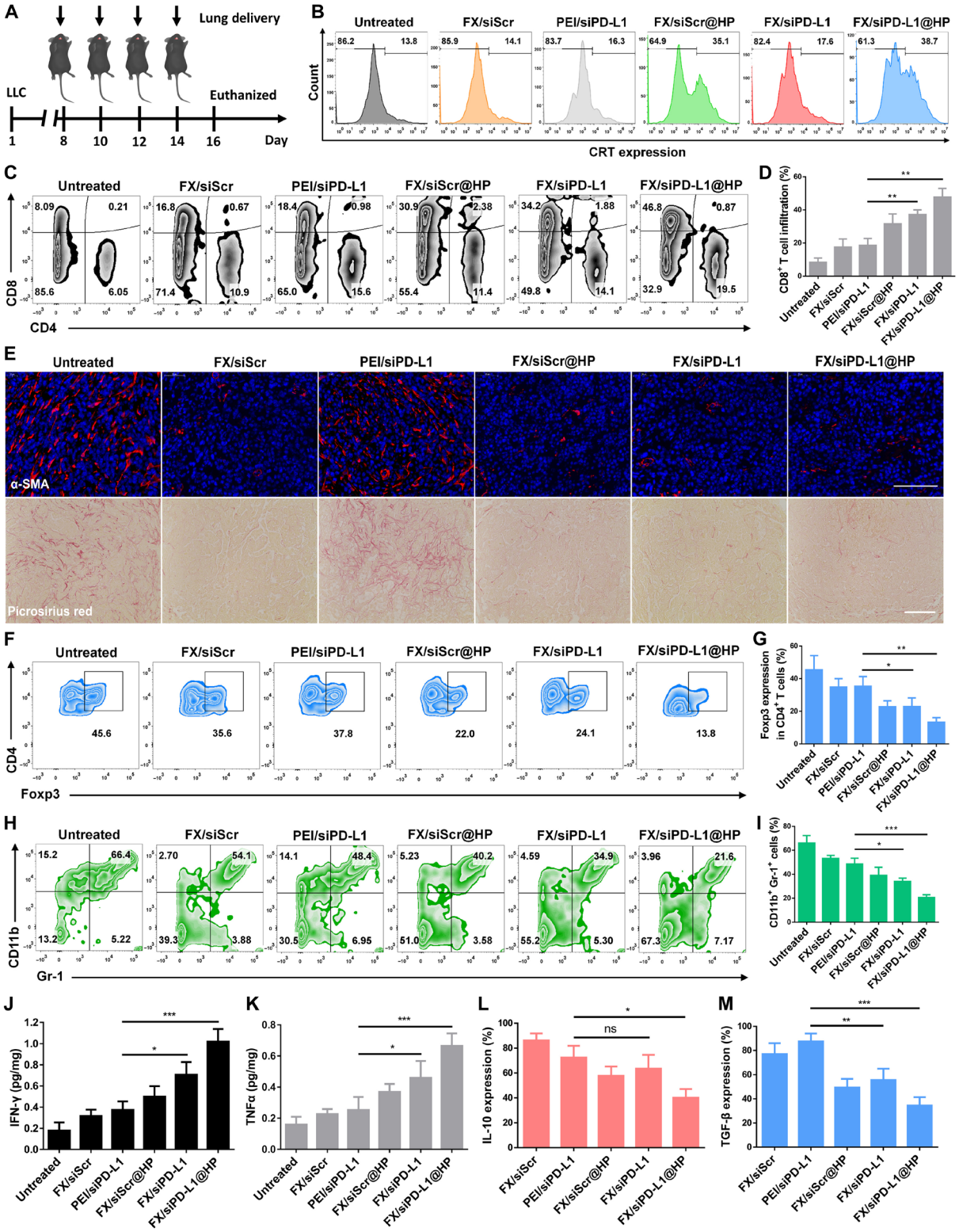

Fig. 6. Antitumor mechanism in vivo. (**A**) After implantation of LLC cells, the treatments were given on days 8, 10, 12, and 14, and the mice were euthanized to collect the tumors on day 16 for further analysis. (**B**) CRT exposure of LLC cells. (**C** and **D**) Percentages and representative flow cytometry plots of $CD4^+$ and $CD8^+$ T cells in tumors. (**E**) α-SMA immunofluorescence staining and picrosirius red staining of the collected tumors after different treatments (scale bars, 100 μm). (**F** and **G**) Percentages and representative flow cytometry plots of T_{regs} in tumors. (**H** and **I**) Percentages and representative flow cytometry plots of MDSCs in tumors. (**J**) IFN-γ and (**K**) TNFα expression detected by ELISA. (**L**) IL-10 and (**M**) TGF-β expression analyzed by immunofluorescence staining. The IL-10 expression and TGF-β expression of the untreated group were set as 100%. Data were analyzed with unpaired *t* test, $^*P < 0.05$, $^{**}P < 0.01$, $^{***}P < 0.001$, ns. not significant.

been one of the most intractable difficulties in ICB therapy. Recent studies show that the presence of a dense desmoplasia (or fibrosis) in tumor constitutes an immunosuppressive barrier for T cell infiltration and is closely related to the therapeutic failure of ICB therapy. CXCR4 is highly expressed in many tumors and plays an important role for both the fibrosis and immune suppression in the TME. Inhibition of CXCR4 with plerixafor (AMD3100) decreases desmoplasia, reduces immunosuppression, and improves T cell infiltration and response to ICB (*33*). To overcome the limitations and increase the response rate of anti–PD-L1 therapy, we developed a CXCR4 antagonistic nanosystem for the delivery of anti–PD-L1 inhibitors and demonstrated its superiority in the treatment of LLC and LMBC (Figs. 4G and 5E). Minimal T lymphocyte infiltration was found in tumors resistant to anti–PD-L1 immunotherapy, which is largely attributed to the fibrotic state in the TME. We further clarify that the designed CXCR4 antagonistic nanoparticles can decrease the fibrosis to increase the effector T cell infiltration in the tumor, which will subsequently enhance the anti–PD-1/PD-L1 immunotherapy (Fig. 6, C and D).

Adequate T cell infiltration can provide enough soldiers to kill tumor cells for the anti–PD-1/PD-L1 immunotherapy. However, just enough soldiers cannot guarantee a good win in the battle against cancer. DCs are the commanders and dominate various functions of the immune system. The main function of DCs is to phagocytize, process, and present antigens and to tell effector T cells about the characteristics of cancer cells. Therefore, successful anti–PD-1/PD-L1 immunotherapy requires a close interaction between effector T cells and DCs, which can turn T cells soldiers into elite troops and provide enough information about the enemy (*34*). Accurate recognition of tumor cells and effective antigen presentation are the key to ensure the immune response. We found that the nanocomplex could increase the CRT exposure on the tumor cell (Figs. 3C and 6B) for better activation of DCs, which worked together with the PD-L1 silence to achieve potent antitumor immune response.

Given the immunosuppressive effects, elimination of MDSCs and T_{regs} may help enhance the immune response and rebuild the immune surveillance in TME. CXCL12/CXCR4 and CXCL5/CXCR2 are closely involved in the recruitment of Gr-1^+CD11b^+ cells into TME (*35*). Moreover, T_{regs} and plasmacytoid DCs (pDCs), which help the immune escape of cancer cells, are also attracted to the TME through the CXCL12/CXCR4 axis. By recruiting and retaining these immunosuppressive cells, the TME limits the effectiveness of immune responses (*36*, *37*). We suggest that reducing the recruitment of MDSCs and T_{regs} in the TME might help the anti–PD-1/PD-L1 immunotherapy. Immunosuppressive cells such as T_{regs} and MDSCs secrete TGF-β, which can inhibit the proliferation and differentiation of various immune cells in tumor tissues and inhibit the immune response through a series of mechanisms. Co-delivery of PD-L1–inhibiting and TGF-β–blocking antibodies reduced TGF-β in the TME, facilitated T cell tumor penetration, and provoked enhanced immune response and better antitumor effects (*38*–*40*). TGF-β attenuates tumor response to PD-L1 inhibition through contributing to exclusion of T cells. Also, the expression of TGF-β and IL-10 is closely related to T_{regs} and MDSCs infiltration in the TME, which is mainly controlled by the CXCR4/CXCL12 axis (*41*, *42*). Both the released PTX and the CXCR4 antagonistic polymer in the nanocomplex selectively decreased the number of T_{regs} and MDSCs (Fig. 6, F to I), thus achieving a low expression of immunosuppressive cytokines IL-10 and TGF-β (Fig. 6, L and M). We believe that helped the nanocomplex to relieve the immunosuppressive state and rebuild the all-around and multilevel immune surveillance.

CONCLUSIONS

In conclusion, we have successfully developed a CXCR4 antagonistic immunoregulatory nanocomplex (FX/siPD-L1@HP) to enhance the anti–PD-L1 immunotherapy for the treatment of LLC and LMBC. The nanocomplex was administered by pulmonary delivery to ensure the adequate interaction with TME. Regulation of antitumor immune process to enhance anti–PD-L1 immunotherapy was achieved by increasing T cell infiltration, promoting the exposure of CRT on tumors, and decreasing the MDSCs and T_{regs} in the TME. CRT exposure promotes the antigen presentation and maturation of DCs to strengthen positive regulation of the immune process. In addition, reduction of MDSCs and T_{regs} inhibits the secretion of TGF-β and IL-10 to attenuate the negative regulation of immune process. Also, CXCR4 inhibition by the nanocomplex decreased the tumor fibrosis and facilitated CTL penetration to further enhance anti–PD-L1 immune response. Overall, the CXCR4-inhibiting nanocomplex regulates the antitumor immune response process and overcomes therapeutic resistance to anti–PD-L1 immunotherapy.

MATERIALS AND METHODS

Materials and cell lines

Heptafluorobutyric anhydride (HFBA) and cystaminebisacrylamide (CBA) were from Sigma-Aldrich. AMD3100 was purchased from Biochempartner Inc. (Shanghai, China). SDF-1 was from PeproTech Inc. (USA). Negative control siRNA (siScr, sense strand, 5′-UUC UCC GAA CGU GUC ACG UTT-3′), siRNA targeting PD-L1 (sense strand, 5′-CCC ACA UAA AAA ACA GUU GTT-3′), and FAM- and Cy5-labeled siScr were from GenePharma (Shanghai, China). Luciferase assay kit and BCA protein assay kit were from the Beyotime Institute of Biotechnology. Monoclonal antibodies anti–PD-L1 and anti-CRT were from Abcam (Cambridge, UK). Anti-CD11c, anti-CD40, anti-CD86, anti-CD45, anti-CD3, anti-CD4, anti-CD8, anti-CD25, anti-Foxp3, anti-CD11b, anti–Gr-1, and transcription factor buffer set were from BD Biosciences. IFN-γ and TNFα enzyme-linked immunosorbent assay (ELISA) kit were from MultiSciences (Lianke) Biotech Co. Ltd. Trypsin, penicillin, streptomycin, Dulbecco's modified Eagle's medium (DMEM), RPMI 1640, PBS, and fetal bovine serum (FBS) were from Gibco (Thermo Fisher Scientific, USA). Human epithelial osteosarcoma U2OS cells stably expressing functional EGFP-CXCR4 fusion protein were purchased from Thermo Fisher Scientific and cultured in DMEM supplemented with 2 mM L-glutamine, 1% penicillin-streptomycin, G418 (0.5 mg/ml), and 10% FBS. Mouse LLC cells were purchased from the American Type Culture Collection and cultured in RPMI 1640 supplemented with 10% FBS. 4T1.Luc cells were from PerkinElmer and cultured in RPMI 1640 with 10% FBS. All the cells were maintained at a 37°C incubator with 5% CO_2.

Synthesis of FX and preparation of FX@HP

Reducible polymeric CXCR4 antagonist RX was synthesized by Michael addition copolymerization of a reducible bisacrylamide CBA using the method as previously reported (*22*, *23*). Briefly, in a typical polymerization reaction, a Boc-protected cyclam monomer (76.3 mg,

0.1 mmol) and CBA (26 mg, 0.1 mmol) were dissolved in 0.7 ml of methanol/water (7/3 v/v), and the polymerization was carried out at 50°C for 14 days. Then, another 4 mg of cyclam was added, stirring for an additional 2 days. After isolating by evaporation, the protecting Boc groups were removed by stirring in trifluoroacetic acid/dichloromethane solution overnight. The product was further evaporated, dissolved in acidified water (pH 4), and dialyzed against acidified water (pH 4) using dialysis membrane with a molecular weight cutoff (MWCO) of 1 kDa. Lyophilization was used to obtain the final product RX. Then, RX (30 mg) was dissolved in 2 ml of methanol and mixed with methanol solution of HFBA (4.1 mg, 0.01 mmol). Triethylamine (1.7 μl, 0.02 mmol) was added and the reaction mixture was stirred at room temperature under nitrogen in the dark for 48 hours. The mixture was diluted into water (pH 4, HCl) and dialyzed (MWCO, 1 kDa) against water for 2 days before final lyophilization to obtain FX.

As previously reported (*43*, *44*), HSA was dissolved in 50 ml of ultrapure water with constant stirring at 37°C, and 100 μl of DTT (10 mg/ml) was added. After 15 min, PTX (10 mg/ml, ethanol as solvent) was added. The HSA-PTX aqueous suspension was extensively dialyzed with membrane (MWCO, 8 kDa) to remove any remnant DTT before lyophilization. FX was added into the HSA-PTX aqueous suspension before it was mixed with a pipette and further sonicated with a sonicator. The FX@HP aqueous suspension was further kept at 4°C after ultrafiltration.

Preparation and characterization of siRNA polyplexes

To prepare the polyplexes, RX, FX, and FX@HP were added to the solution of siRNA (20 μg/ml) in 10 mM Hepes. The polyplexes were then vortexed for 1 min and left standing at room temperature for 30 min before use. Hydrodynamic size and ζ potential of the polyplexes were measured by Zeta Plus (Zetasizer Nano S90, Malvern). Particle morphology was observed using transmission electron microscopy (H-600, Hitachi, Japan). The siRNA binding ability was evaluated by agarose gel electrophoresis. The polyplexes were prepared at FX/siRNA w/w ratios 0 to 6 and mixed with RNA-loading buffer before running on a 1% agarose gel (100 V, 15 min) stained with GelRed. The siRNA bands were visualized using ultraviolet (UV) illumination.

In vitro drug release from the nanocomplex

A predetermined amount of the PTX-loaded nanocomplex was redispersed in 2 ml of tris buffer (5 mM, pH 7.2) with or without GSH (10 mM) and then closed into a dialysis bag (MWCO, 3.5 kDa). Then, the bag was immersed into 10 ml of release buffer (tris solution containing 9% ethanol, v/v). At a certain time, the release buffer was withdrawn for HPLC analysis, and the same volume of releasing buffer was added. For the HPLC assay, UV/Vis detection at 227 nm and a C-18 reverse-phase column (Kromasil, 5 μm, 4.6 mm by 250 mm) were used for the analysis of PTX. The column was equilibrated with acetonitrile-water (50:50 v/v) for 15 min. The mobile phase was acetonitrile-water (60:40 v/v). The flow rate was 1 ml min^{-1}. The siRNA polyplexes were made as previously described before they are treated with GSH for 45 min and the siRNA release was analyzed by the agarose gel electrophoresis.

Cell uptake and PD-L1 silencing in vitro

Cellular uptake of the polyplexes (FAM-siRNA) was determined in LLC cells cultured in 12-well plates. Polyplexes were added to a 12-well plate for 4 hours of incubation. Flow cytometry assay of the cell uptake was performed for the collected cells. The LLC cells (6×10^6) were seeded 12 hours before the treatment in a six-well plate. After washing with PBS, the transfection procedure with siPD-L1 (100 nM) polyplexes was performed as described above. After 48 hours, total protein was extracted and quantified with the BCA kit before it was separated by SDS–polyacrylamide gel electrophoresis. The samples were transferred to nitrocellulose membrane, followed by probing with PD-L1 and β-actin antibodies and incubation with horseradish peroxidase–linked secondary antibody at 37°C for 1 hour. Quantification of the band intensities was performed using ImageJ.

CXCR4 antagonism

CXCR4 antagonism of polyplexes was measured using a protocol described in detail previously (*23*). Briefly, U2OS cells stably expressing functional EGFP-CXCR4 fusion protein were treated with polyplexes or AMD3100 (300 nM) for 30 min and 10 nM SDF-1α was added for 1 hour. Cells were then washed three times with PBS and fixed with 4% paraformaldehyde for 20 min before they were photographed using an EVOS FL microscope.

CRT exposure and DC maturation in vitro

LLC cells were seeded into confocal dishes and treated with the nanocomplex (100 nM siPD-L1 and 100 nM PTX) for 24 hours. Then, the cells were washed with PBS and incubated with anti-CRT antibody. After that, the CRT exposure was observed using laser scanning confocal microscopy and detected by flow cytometry assay.

Bone marrow cells were obtained from C57BL/6 mice with a syringe according to the method described before (*45*). After 4 to 6 hours of culture, the nonadherent cells were removed, and the adherent cells were plated in a six-well plate (10^6 cells each well), induced to differentiate into DCs by adding IL-4 (20 ng/ml) and granulocyte macrophage colony-stimulating factor (20 ng/ml). Half of the medium was changed every 2 days. On day 4, cell differentiation into DCs was confirmed by CD11c staining. The nanocomplex (100 nM siPD-L1 and 100 nM PTX) and the tumor cells (10^6 cells each well) were added on day 4. On day 7, DCs were collected for the flow cytometry assay to detect CD40 and CD86 expression.

Biodistribution and in vivo antitumor efficacy

The orthotopic LLC model was established according to previous reports (*46*, *47*). Briefly, chests of the C57BL/6 mice were shaved. The mice were anesthetized with pentobarbital sodium (5 mg/kg). At 1 cm below the axillary front, the skin was lifted with tweezers and about 1 cm was cut with ophthalmic scissors. Next, LLC cell suspension containing precooled Matrigel (1.35 mg/ml) was injected into the lung with a 5- to 10-s stop after the injection. The incision was closed using veterinary skin adhesive. On day 8, mice with orthotopic LLC were given a single dose of the nanocomplex prepared with siScr-Cy5 [siRNA (0.8 mg/kg), w/w 5] by intratracheal instillation. Fluorescence imaging (excitation/emission, 640/680 nm) was done on IVIS Lumina (Xenogen Co., USA). Images were acquired 1 to 24 hours after administration. The amount of siScr-Cy5 in tissues was analyzed with IVIS Living Imaging Software.

All animal experiments followed regulations of the Institutional Animal Care and Use Committee of China Pharmaceutical University and protocols were approved by the Science and Technology Department of Jiangsu Province. After the establishment of the mouse orthotopic lung cancer model as described above, treatments were administered by intratracheal instillation on days 8, 10, 12, 14, 16, and 18, and the survival was monitored to day 60. During pulmonary

delivery, the nanocomplex was prepared as previously described in a volume of 40 μl in PBS before intratracheal instillation. Each mouse received siRNA (0.8 mg/kg) and PTX (1 mg/kg).

The LMBC model was established by tail vein injection of 4T1. Luc cells. On day 8, the lung metastasis formation was confirmed by bioluminescence imaging. Different treatments were given by intratracheal instillation in a volume of 40 μl [PTX (1 mg/kg) and siRNA (0.8 mg/kg)] on days 8, 10, 12, and 14, and the bioluminescence imaging was performed on days 8, 12, and 16. The lungs were harvested on day 16 and fixed in Bouin's solution overnight and then stored in 70% ethanol. H&E assay was performed by Wuhan Servicebio Technology. For the survival analysis, different treatments were given on days 8, 10, 12, 14, 16, and 18, and the survival was monitored to day 55.

Analysis of the TME

The LLC-bearing mice were administered by pulmonary delivery on days 8, 10, 12, and 14, and the tumors were collected on day 16. Tumor tissues were fixed for 24 hours in 4% paraformaldehyde and sent out to Wuhan Servicebio Technology for subsequent staining. The PD-L1 expression was analyzed by immunohistochemistry staining. The CXCR4 expression, $CD8^+$ T cell infiltration, α-SMA expression, and IL-10 and TGF-β expression were analyzed by immunofluorescence staining. Slides were mounted with Vectashield Mounting Media containing 4′,6-diamidino-2-phenylindole before they were analyzed under a fluorescence microscope. For the CRT expression, tumor tissues were collected and homogenized in cold saline. The tumor cells were incubated with anti-CRT for 1 hour before they were detected with the flow cytometry assay. Infiltrating lymphocytes in tumors were obtained according to the standard protocols with Percoll (GE). For the T cell and T_{reg} detection, the collected lymphocytes were incubated with anti–CD45-FITC, anti–CD3-BB700, anti–CD8-PE-Cy7, anti–CD4-APC, anti–CD25-BV421, and anti–Foxp3-PE and detected by flow cytometry (BD FACSVerse, USA) according to the standard protocols. For the MDSC detection, the collected lymphocytes were incubated with anti–CD45-FITC, anti–CD11b-Percp-Cy5.5, and anti–Gr-1-PE and detected by the flow cytometry assay according to the standard protocols. The infiltrating IFN-γ and TNFα were measured by an ELISA kit according to the instructions.

Statistical analysis

All data were representative results from at least three independent experiments. Results are shown as means ± SD. The *t* test was used to determine the statistical significance. All statistical analysis was performed with GraphPad Prism v6.

SUPPLEMENTARY MATERIALS

Supplementary material for this article is available at http://advances.sciencemag.org/cgi/content/full/6/20/eaaz9240/DC1

View/request a protocol for this paper from *Bio-protocol*.

REFERENCES AND NOTES

1. J. R. Brahmer, S. S. Tykodi, L. Q. M. Chow, W. J. Hwu, S. L. Topalian, P. Hwu, C. G. Drake, L. H. Camacho, J. Kauh, K. Odunsi, H. C. Pitot, O. Hamid, S. Bhatia, R. Martins, K. Eaton, S. M. Chen, T. M. Salay, S. Alaparthy, J. F. Grosso, A. J. Korman, S. M. Parker, S. Agrawal, S. M. Goldberg, D. M. Pardoll, A. Gupta, J. M. Wigginton, Safety and activity of anti-PD-L1 antibody in patients with advanced cancer. *N. Engl. J. Med.* **366**, 2455–2465 (2012).
2. A. Ribas, J. D. Wolchok, Cancer immunotherapy using checkpoint blockade. *Science* **359**, 1350–1355 (2018).
3. W. Zou, J. D. Wolchok, L. Chen, PD-L1 (B7-H1) and PD-1 pathway blockade for cancer therapy: Mechanisms, response biomarkers, and combinations. *Sci. Transl. Med.* **8**, 328rv4 (2016).
4. Y. Chao, L. G. Xu, C. Liang, L. Z. Feng, J. Xu, Z. L. Dong, L. L. Tian, X. Yi, K. Yang, Z. Liu, Combined local immunostimulatory radioisotope therapy and systemic immune checkpoint blockade imparts potent antitumour responses. *Nat. Biomed. Eng.* **2**, 611–621 (2018).
5. C. Wang, W. Sun, Y. Ye, Q. Hu, H. N. Bomba, Z. Gu, In situ activation of platelets with checkpoint inhibitors for post-surgical cancer immunotherapy. *Nat. Biomed. Eng.* **1**, 0011 (2017).
6. P. Sharma, J. P. Allison, The future of immune checkpoint therapy. *Science* **348**, 56–61 (2015).
7. P. S. Hegde, V. Karanikas, S. Evers, The where, the when, and the how of immune monitoring for cancer immunotherapies in the era of checkpoint inhibition. *Clin. Cancer Res.* **22**, 1865–1874 (2016).
8. M. Katoh, M. Katoh, Integrative genomic analyses of CXCR4: Transcriptional regulation of CXCR4 based on TGFβ, nodal, activin signaling and POU5F1, FOXA2, FOXC2, FOXH1, SOX17, and GFI1 transcription factors. *Int. J. Oncol.* **36**, 415–420 (2010).
9. M. C. B. Tan, P. S. Goedegebuure, B. A. Belt, B. Flaherty, N. Sankpal, W. E. Gillanders, T. J. Eberlein, C. S. Hsieh, D. C. Linehan, Disruption of CCR5-dependent homing of regulatory T cells inhibits tumor growth in a murine model of pancreatic cancer. *J. Immunol.* **182**, 1746–1755 (2009).
10. T. A. Mace, Z. Ameen, A. Collins, S. Wojcik, M. Mair, G. S. Young, J. R. Fuchs, T. D. Eubank, W. L. Frankel, T. Bekaii-Saab, M. Bloomston, G. B. Lesinski, Pancreatic cancer-associated stellate cells promote differentiation of myeloid-derived suppressor cells in a STAT3-dependent manner. *Cancer Res.* **73**, 3007–3018 (2013).
11. R. L. Sleightholm, B. K. Neilsen, J. Li, M. M. Steele, R. K. Singh, M. A. Hollingsworth, D. Oupicky, Emerging roles of the CXCL12/CXCR4 axis in pancreatic cancer progression and therapy. *Pharmacol. Ther.* **179**, 158–170 (2017).
12. D. E. Large, J. R. Soucy, J. Hebert, D. T. Auguste, Advances in receptor-mediated, tumor-targeted drug delivery. *Adv. Ther.* **2**, 1800091 (2018).
13. B. Mehrad, M. D. Burdick, R. M. Strieter, Fibrocyte CXCR4 regulation as a therapeutic target in pulmonary fibrosis. *Int. J. Biochem. Cell Biol.* **41**, 1708–1718 (2009).
14. J. Xu, A. Mora, H. Shim, A. Stecenko, K. L. Brigham, M. Rojas, Role of the SDF-1/CXCR4 axis in the pathogenesis of lung injury and fibrosis. *Am. J. Respir. Cell Mol. Biol.* **37**, 291–299 (2007).
15. Y. Chen, R. Xia, Y. Huang, W. Zhao, J. Li, X. Zhang, P. Wang, R. Venkataramanan, J. Fan, W. Xie, X. Ma, B. Lu, S. Li, An immunostimulatory dual-functional nanocarrier that improves cancer immunochemotherapy. *Nat. Commun.* **7**, 13443 (2016).
16. A. M. Cook, W. J. Lesterhuis, A. K. Nowak, R. A. Lake, Chemotherapy and immunotherapy: Mapping the road ahead. *Curr. Opin. Immunol.* **39**, 23–29 (2016).
17. Q. L. Song, Y. J. Yin, L. H. Shang, T. T. Wu, D. Zhang, M. Kong, Y. D. Zhao, Y. Z. He, S. W. Tan, Y. Y. Guo, Z. P. Zhang, Tumor microenvironment responsive nanogel for the combinatorial antitumor effect of chemotherapy and immunotherapy. *Nano Lett.* **17**, 6366–6375 (2017).
18. H. Zhong, B. H. Han, I. L. Tourkova, A. Lokshin, A. Rosenbloorn, M. R. Shurin, G. V. Shurin, Low-dose paclitaxel prior to intratumoral dendritic cell vaccine modulates intratumoral cytokine network and lung cancer growth. *Clin. Cancer Res.* **13**, 5455–5462 (2007).
19. L. Galluzzi, A. Buqué, O. Kepp, L. Zitvogel, G. Kroemer, Immunological effects of conventional chemotherapy and targeted anticancer agents. *Cancer Cell* **28**, 690–714 (2015).
20. M. Tagliamonte, A. Petrizzo, M. Napolitano, A. Luciano, D. Rea, A. Barbieri, C. Arra, P. Maiolino, M. Tornesello, G. Ciliberto, F. M. Buonaguro, L. Buonaguro, A novel multi-drug metronomic chemotherapy significantly delays tumor growth in mice. *J. Transl. Med.* **14**, 58 (2016).
21. J. Li, Y. Zhu, S. T. Hazeldine, C. Li, D. Oupicky, Dual-function CXCR4 antagonist polyplexes to deliver gene therapy and inhibit cancer cell invasion. *Angew. Chem. Int. Ed. Engl.* **51**, 8740–8743 (2012).
22. Y. Wang, S. T. Hazeldine, J. Li, D. Oupicky, Development of functional poly(amido amine) CXCR4 antagonists with the ability to mobilize leukocytes and deliver nucleic acids. *Adv. Healthc. Mater.* **4**, 729–738 (2015).
23. Y. Wang, S. Kumar, S. Rachagani, B. R. Sajja, Y. Xie, Y. Hang, M. Jain, J. Li, M. D. Boska, S. K. Batra, D. Oupicky, Polyplex-mediated inhibition of chemokine receptor CXCR4 and chromatin-remodeling enzyme NCOA3 impedes pancreatic cancer progression and metastasis. *Biomaterials* **101**, 108–120 (2016).
24. M. M. Wang, H. M. Liu, L. Li, Y. Y. Cheng, A fluorinated dendrimer achieves excellent gene transfection efficacy at extremely low nitrogen to phosphorus ratios. *Nat. Commun.* **5**, 3053 (2014).
25. J. Fucikova, E. Becht, K. Iribarren, J. Goc, R. Remark, D. Damotte, M. Alifano, P. Devi, J. Biton, C. Germain, A. Lupo, W. H. Fridman, M. C. Dieu-Nosjean, G. Kroemer, C. Sautés-Fridman, I. Cremer, Calreticulin expression in human non-small cell lung cancers correlates

with increased accumulation of antitumor immune cells and favorable prognosis. *Cancer Res.* **76**, 1746–1756 (2016).
26. M. Katsura, F. Shoji, T. Okamoto, S. Shimamatsu, F. Hirai, G. Toyokawa, Y. Morodomi, T. Tagawa, Y. Oda, Y. Maehara, Correlation between CXCR4/CXCR7/CXCL12 chemokine axis expression and prognosis in lymph-node-positive lung cancer patients. *Cancer Sci.* **109**, 154–165 (2018).
27. I. Martins, O. Kepp, L. Galluzzi, L. Senovilla, F. Schlemmer, S. Adjemian, L. Menger, M. Michaud, L. Zitvogel, G. Kroemer, Surface-exposed calreticulin in the interaction between dying cells and phagocytes. *Ann. N. Y. Acad. Sci.* **1209**, 77–82 (2010).
28. V. Bronte, E. Apolloni, A. Cabrelle, R. Ronca, P. Serafini, P. Zamboni, N. P. Restifo, P. Zanovello, Identification of a $CD11b^+/Gr\text{-}1^+/CD31^+$ myeloid progenitor capable of activating or suppressing $CD8^+$ T cells. *Blood* **96**, 3838–3846 (2000).
29. E. Suzuki, V. Kapoor, A. S. Jassar, L. R. Kaiser, S. M. Albelda, Gemcitabine selectively eliminates splenic $Gr\text{-}1^+/CD11b^+$ myeloid suppressor cells in tumor-bearing animals and enhances antitumor immune activity. *Clin. Cancer Res.* **11**, 6713–6721 (2005).
30. M. Ahmadzadeh, A. Pasetto, L. Jia, D. C. Deniger, S. Stevanović, P. F. Robbins, S. A. Rosenberg, Tumor-infiltrating human $CD4^+$ regulatory T cells display a distinct TCR repertoire and exhibit tumor and neoantigen reactivity. *Sci. immunol.* **4**, eaao4310 (2019).
31. T. Maj, W. Wang, J. Crespo, H. Zhang, W. Wang, S. Wei, L. Zhao, L. Vatan, I. Shao, W. Szeliga, C. Lyssiotis, J. R. Liu, I. Kryczek, W. Zou, Oxidative stress controls regulatory T cell apoptosis and suppressor activity and PD-L1-blockade resistance in tumor. *Nat. Immunol.* **18**, 1332–1341 (2017).
32. L. Delamarre, The immunotherapy prize! *Sci. Adv.* **4**, eaat7955 (2018).
33. I. X. Chen, V. P. Chauhan, J. Posada, M. R. Ng, M. W. Wu, P. Adstamongkonkul, P. Huang, N. Lindeman, R. Langer, R. K. Jain, Blocking CXCR4 alleviates desmoplasia, increases T-lymphocyte infiltration, and improves immunotherapy in metastatic breast cancer. *Proc. Natl. Acad. Sci. U.S.A.* **116**, 4558–4566 (2019).
34. C. S. Garris, S. P. Arlauckas, R. H. Kohler, M. P. Trefny, S. Garren, C. Piot, C. Engblom, C. Pfirschke, M. Siwicki, J. Gungabeesoon, G. J. Freeman, S. E. Warren, S. Ong, E. Browning, C. G. Twitty, R. H. Pierce, M. H. Le, A. P. Algazi, A. I. Daud, S. I. Pai, A. Zippelius, R. Weissleder, M. J. Pittet, Successful anti-PD-1 cancer immunotherapy requires T cell-dendritic cell crosstalk involving the cytokines IFN-γ and IL-12. *Immunity* **49**, 1148–1161.e7 (2018).
35. L. Yang, J. Huang, X. Ren, A. E. Gorska, A. Chytil, M. Aakre, D. P. Carbone, L. M. Matrisian, A. Richmond, P. C. Lin, H. L. Mosesl, Abrogation of TGF β signaling in mammary carcinomas recruits Gr-1+CD11b+ myeloid cells that promote metastasis. *Cancer Cell* **13**, 23–35 (2008).
36. W. Zou, V. Machelon, A. Coulomb-L'Hermin, J. Borvak, F. Nome, T. Isaeva, S. Wei, R. Krzysiek, I. Durand-Gasselin, A. Gordon, T. Pustilnik, D. T. Curiel, P. Galanaud, F. Capron, D. Emilie, T. J. Curiel, Stromal-derived factor-1 in human tumors recruits and alters the function of plasmacytoid precursor dendritic cells. *Nat. Med.* **7**, 1339–1346 (2001).
37. W. Zou, Regulatory T cells, tumour immunity and immunotherapy. *Nat. Rev. Immunol.* **6**, 295–307 (2006).
38. S. Mariathasan, S. J. Turley, D. Nickles, A. Castiglioni, K. Yuen, Y. Wang, E. E. Kadel III, H. Koeppen, J. L. Astarita, R. Cubas, S. Jhunjhunwala, R. Banchereau, Y. Yang, Y. Guan, C. Chalouni, J. Ziai, Y. Şenbabaoğlu, S. Santoro, D. Sheinson, J. Hung, J. M. Giltnane, A. A. Pierce, K. Mesh, S. Lianoglou, J. Riegler, R. A. D. Carano, P. Eriksson, M. Höglund, L. Somarriba, D. L. Halligan, M. S. van der Heijden, Y. Loriot, J. E. Rosenberg, L. Fong, I. Mellman, D. S. Chen, M. Green, C. Derleth, G. D. Fine, P. S. Hegde, R. Bourgon, T. Powles, TGFβ attenuates tumour response to PD-L1 blockade by contributing to exclusion of T cells. *Nature* **554**, 544–548 (2018).
39. D. V. F. Tauriello, S. Palomo-Ponce, D. Stork, A. Berenguer-Llergo, J. Badia-Ramentol, M. Iglesias, M. Sevillano, S. Ibiza, A. Cañellas, X. Hernando-Momblona, D. Byrom, J. A. Matarin, A. Calon, E. I. Rivas, A. R. Nebreda, A. Riera, C. S. Attolini, E. Batlle, TGFβ drives immune evasion in genetically reconstituted colon cancer metastasis. *Nature* **554**, 538–543 (2018).
40. Y. Lan, D. Zhang, C. X. Xu, K. W. Hance, B. Marelli, J. Qi, H. K. Yu, G. Z. Qin, A. Sircar, V. M. Hernández, M. H. Jenkins, R. E. Fontana, A. Deshpande, G. Locke, H. Sabzevari, L. Radvanyi, K. M. Lo, Enhanced preclinical antitumor activity of M7824, a bifunctional fusion protein simultaneously targeting PD-L1 and TGF-β. *Sci. Transl. Med.* **10**, eaan5488 (2018).
41. H. Tang, Y. Wang, L. K. Chlewicki, Y. Zhang, J. Guo, W. Liang, J. Wang, X. Wang, Y. X. Fu, Facilitating T cell infiltration in tumor microenvironment overcomes resistance to PD-L1 blockade. *Cancer Cell* **30**, 500 (2016).
42. E. Eriksson, J. Wenthe, S. Irenaeus, A. Loskog, G. Ullenhag, Gemcitabine reduces MDSCs, tregs and TGFβ-1 while restoring the teff/treg ratio in patients with pancreatic cancer. *J. Transl. Med.* **14**, 282 (2016).
43. G. Gong, Y. Xu, Y. Zhou, Z. Meng, G. Ren, Y. Zhao, X. Zhang, J. Wu, Y. Hu, Molecular switch for the assembly of lipophilic drug incorporated plasma protein nanoparticles and in vivo image. *Biomacromolecules* **13**, 23–28 (2012).
44. J. Wu, C. Song, C. Jiang, X. Shen, Q. Qiao, Y. Hu, Nucleolin targeting AS1411 modified protein nanoparticle for antitumor drugs delivery. *Mol. Pharm.* **10**, 3555–3563 (2013).
45. A. Shintani, N. Nakao, K. Kakishita, T. Itakura, Generation of dopamine neurons from embryonic stem cells in the presence of the neuralizing activity of bone marrow stromal cells derived from adult mice. *J. Neurosci. Res.* **86**, 2829–2838 (2008).
46. H. Y. Li, M. McSharry, B. Bullock, T. T. Nguyen, J. Kwak, J. M. Poczobutt, T. R. Sippel, L. E. Heasley, M. C. Weiser-Evans, E. T. Clambey, R. A. Nemenoff, The tumor microenvironment regulates sensitivity of murine lung tumors to PD-1/PD-L1 antibody blockade. *Cancer Immunol. Res.* **5**, 767–777 (2017).
47. Y. Zou, M. Zheng, W. Yang, F. Meng, K. Miyata, H. J. Kim, K. Kataoka, Z. Zhong, Virus-mimicking chimaeric polymersomes boost targeted cancer siRNA therapy in vivo. *Adv. Mater.* **29**, 1703285 (2017).

Acknowledgments
Funding: This work was supported by the National Key Research and Development Program of China (no. 2017YFA0205402), the Science Fund for Distinguished Young Scholars of Jiangsu Province, China (no. BK20170028), the China National Science Foundation (81573377 and 81872817), the "Double First-Class" University Project of China Pharmaceutical University (CPU2018GY07), the Changjiang Scholar Program, and a start-up fund from the University of Nebraska Medical Center. **Author contributions:** Concept and design: D.O., M.S., and Z.L.; experimental operation: Z.L., Y.S., and Y.W.; data processing: Z.L. and Y.W.; writing and revision: Z.L., C.Q., D.O., and M.S. **Competing interests:** The authors declare that they have no competing interests. **Data and materials availability:** All data needed to evaluate the conclusions in the paper are present in the paper and/or the Supplementary Materials. Additional data related to this paper may be requested from the authors.

Submitted 21 October 2019
Accepted 2 March 2020
Published 15 May 2020
10.1126/sciadv.aaz9240

Citation: Z. Li, Y. Wang, Y. Shen, C. Qian, D. Oupicky, M. Sun, Targeting pulmonary tumor microenvironment with CXCR4-inhibiting nanocomplex to enhance anti–PD-L1 immunotherapy. *Sci. Adv.* **6**, eaaz9240 (2020).